

AperTO - Archivio Istituzionale Open Access dell'Università di Torino

Photo-oxidative degradation of toluene in aqueous media by hydroxyl radicals

This is the author's manuscript

Original Citation:

Availability:

This version is available <http://hdl.handle.net/2318/79117> since

Published version:

DOI:10.1016/j.photochem.2010.07.021

Terms of use:

Open Access

Anyone can freely access the full text of works made available as "Open Access". Works made available under a Creative Commons license can be used according to the terms and conditions of said license. Use of all other works requires consent of the right holder (author or publisher) if not exempted from copyright protection by the applicable law.

(Article begins on next page)



UNIVERSITÀ DEGLI STUDI DI TORINO

This Accepted Author Manuscript (AAM) is copyrighted and published by Elsevier. It is posted here by agreement between Elsevier and the University of Turin. Changes resulting from the publishing process - such as editing, corrections, structural formatting, and other quality control mechanisms - may not be reflected in this version of the text. The definitive version of the text was subsequently published in

A. Hatipoglu, D. Vione, Y. Yalçin, C. Minero, Z. Çinar. Photo-oxidative Degradation of Toluene in Aqueous Media by Hydroxyl Radicals. *J. Photochem. Photobiol. A: Chem.* **2010**, *215*, 59-68.

DOI: 10.1016/j.photochem.2010.07.021.

You may download, copy and otherwise use the AAM for non-commercial purposes provided that your license is limited by the following restrictions:

- (1) You may use this AAM for non-commercial purposes only under the terms of the CC-BY-NC-ND license.
- (2) The integrity of the work and identification of the author, copyright owner, and publisher must be preserved in any copy.
- (3) You must attribute this AAM in the following format:

A. Hatipoglu, D. Vione, Y. Yalçin, C. Minero, Z. Çinar. Photo-oxidative Degradation of Toluene in Aqueous Media by Hydroxyl Radicals. *J. Photochem. Photobiol. A: Chem.* **2010**, *215*, 59-68.

DOI: 10.1016/j.photochem.2010.07.021 (<http://www.elsevier.com/locate/jphotochem>).

Photo-oxidative Degradation of Toluene in Aqueous Media by Hydroxyl Radicals

Arzu HATIPOGLU⁽¹⁾, Davide VIONE⁽²⁾, Claudio MINERO⁽²⁾, Yelda YALÇIN⁽¹⁾,
Zekiye ÇINAR^{(1)*}

(1) Yildiz Technical University, Department of Chemistry, 34220 Istanbul, Turkey

(2) Università di Torino, Dipartimento di Chimica Analitica, Via P.Giuria 5, 10125
Torino, Italy

ABSTRACT

In this study, with the intention of determining the most probable reaction path and the product distribution for the photo-oxidative degradation of toluene in aqueous media, a combination of experimental and quantum mechanical methods were used to elucidate the effect of water solvent on the reaction rate and on the subsequent formation of the primary intermediates. In the experimental part of the study, the formation yields of hydroxylated intermediates and of benzaldehyde were measured by HPLC in the presence of nitrate under UVB irradiation as the $\bullet\text{OH}$ source. Modeling of the reaction paths was performed using density functional theory (DFT) calculations to investigate the most plausible mechanism for the initial $\bullet\text{OH}$ attack and to determine the identities of the primary intermediates. Rate coefficients for all the reaction paths were computed by the Transition State Theory (TST) to obtain the product distribution. The effect of solvent water was investigated by using COSMO as the solvation model. The experimental results combined with DFT calculations indicate that *ortho*-addition yielding *o*-cresol is the dominant reaction path for gas and aqueous media. The presence of a dielectric medium such as water has a stabilizing effect that decreases the overall energy for this mechanism. Finally, the significance for surface waters of the reaction between toluene and $\bullet\text{OH}$ was studied by use of a recently developed photochemical model that foresees the lifetime of a compound upon reaction with $\bullet\text{OH}$, as a function of the reaction rate constant, the chemical composition of the surface water layer and the water column depth.

Keywords: Toluene, hydroxyl radicals, photo-oxidative degradation, DFT calculations, COSMO

*Corresponding author Fax: +90.212.383 4134 E-mail: cinarz@yildiz.edu.tr
Phone: +90.212.383 4179

1. INTRODUCTION

Volatile aromatic compounds constitute an important class of water and air contaminants. They are emitted into the environment from mainly anthropogenic sources such as combustion processes, vehicle emissions and industrial sources, as well as from biogenic processes (Raul Alvarez-Idaboy et al., 2001). Atmospheric photochemical oxidation of aromatics results in ozone and secondary aerosol formation. Recent calculations have shown that in urban areas up to 40% of photochemically produced ozone can be attributed to emissions of aromatics (Bohn, 2001). Furthermore, the degradation reactions of aromatic hydrocarbons yield non-volatile organic compounds that contribute to the formation of secondary organic aerosols. The latter have serious effects on human health and the global climate (Suh et al., 2002). The cited atmospheric reactions also play important roles into the formation of polycyclic aromatic hydrocarbons, particulate matter and soot (Seta et al., 2006; Bekbolet et al., 2009). Therefore, the oxidative degradation mechanisms of aromatic compounds is a current hot research topic.

Toluene is the most abundant volatile aromatic hydrocarbon present in the urban atmosphere. It is a rather common constituent of crude oil and a major component of gasoline. For this reason, it is one of the most important contaminants in urban areas, where it can reach some 10 ppbv levels in polluted air (Bruno et al., 2008) and even 1 ppmv in or near refueling stations (Wixtrom and Brown, 1992). The most important removal pathway of toluene from the atmosphere is the gas-phase reaction with $\bullet\text{OH}$, which mainly yields the hydroxylated derivatives (cresols). The latter are 7-11 times more reactive than toluene toward $\bullet\text{OH}$ and, also being more water-soluble, can be more easily removed from the atmosphere (Atkinson, 1994, and references therein).

Toluene is also present in surface and groundwater, usually because of fuel spills or petroleum production. This pollutant in water has been detected world-wide (Katsumata and Kastenbergh, 1996; Holdway and Heggie, 2000; Arambarri et al., 2004; Karaconji et al., 2006; Soh et al., 2007; Fatta et al., 2007; Robinson et al., 2009). The concentration of toluene in surface waters is usually a fraction of $\mu\text{g L}^{-1}$, but values as high as $\sim 10 \mu\text{g L}^{-1}$ have been described (Fatta et al., 2007). As a volatile organic compound, toluene can undergo partitioning between surface waters and the atmosphere, but additional processes are operational that account for its transformation (Heald et al., 2005). Among such processes, biodegradation is a possible pathway for toluene (Robinson et al., 2009). However, photochemistry is another important transformation route for water-dissolved pollutants (Hoigné, 1990), and the reaction with the hydroxyl radical ($\bullet\text{OH}$) can play a key role in the photosensitized degradation of hardly oxidized aromatic compounds (Brezonik and Fulkerson-Brekken, 1998). In recent years, advanced oxidation processes (AOPs) are being used in order to destroy toluene and other aromatic hydrocarbons in water or air. In

all AOPs, including UV/ozone, UV/hydrogen peroxide and near-UV/titanium dioxide, $\bullet\text{OH}$ radicals are generated upon irradiation. These photogenerated $\bullet\text{OH}$ radicals initiate the degradation reactions of all the aromatic hydrocarbons. The degradation reactions of pollutant molecules may take place through formation of harmful intermediates that are more hazardous than the original compound. Therefore, knowledge on the identities of the intermediates and the reaction products is a necessity in the application of such water and air treatment processes. Although the toluene + $\bullet\text{OH}$ reaction has great importance in various fields of chemistry such as environmental chemistry, atmospheric chemistry and combustion chemistry, its degradation mechanism and product distribution is still uncertain.

The reaction of toluene with $\bullet\text{OH}$ radicals proceeds by three pathways: H-atom abstraction either from the side chain or from the ring, and addition to the aromatic ring. In the addition reactions, hydroxymethylcyclohexadienyl radical is formed. Most of the products are formed in the subsequent reactions of this radical. Experimental studies on the gas phase have shown that around 20% of the hydroxylated adducts are converted to cresols by abstraction of the redundant ring H by molecular oxygen (Bohn, 2001). Of the hydroxylated adducts, *o*-cresol has been reported to be the most abundant (Uc et al., 2000). In the presence of molecular oxygen, the hydroxylated adducts may also yield small oxidation products such as glyoxal, methylglyoxal, butanediol etc., which are formed through ring cleavage. They also form peroxy radicals that undergo intramolecular rearrangement, leading to bicyclic radicals that then yield bicyclic peroxy radicals. On the other hand, in the H-abstraction paths from the methyl group and the ring, a benzyl and a methylphenyl radical are formed, respectively. The benzyl radical yields benzaldehyde through the reaction with O_2 . It has been suggested that H-abstraction from ring carbons is of minor importance, because the C-H bonds of the methyl group are much weaker (ca. 85 kcal.mol⁻¹) than those involving carbon atoms from the ring (ca. 110 kcal.mol⁻¹). While this is most likely to occur at room temperature, the contribution of the ring hydrogens to the abstraction path has been determined to be around 10-20% at high temperature (500-1000 K) (Tully et al., 1981; Uc et al., 2006).

The most important experimental result is that at room temperature the activation energy for the toluene + $\bullet\text{OH}$ reaction is positive, whereas at high temperatures it is negative (Suh et al., 2002). The curved Arrhenius plots for this reaction have been attributed to the competition between different possible reaction paths. The reaction of toluene with $\bullet\text{OH}$ radicals *in vacuo* has also been studied computationally, using either wave-function based or density functional quantum mechanical methods (Uc et al., 2000; Suh et al., 2002; Frankcombe and Smith, 2007). Most of the researchers have investigated the initial attack of the $\bullet\text{OH}$ radicals. Uc et al. (2000) have performed MP2 and DFT methods to examine the addition paths and concluded that pre-reactive complexes are

formed prior to the transition states. They have also studied the possibility of *ipso*-addition to the methyl substituted site and determined that it is energetically more favorable than *ortho*-, *meta*- and *para*-addition paths. However, Suh et al. (2002) have calculated the branching ratios for the four possible addition paths and concluded that *ipso*-addition is of minor importance. Their predicted sequence of the positions for gas phase is *ortho*>*para*>*meta*, which is different from that of the former study. H-abstraction paths have also been studied through the use of MP2 and DFT methods (Uc et al., 2006). The results indicate that ring abstraction paths are negligible at room temperature due to their larger energy barriers than side-chain abstraction paths. Transition State Theory calculations by Seta et al. (Seta et al. 2006) on quantum chemically determined energies have confirmed the dominance of side-chain abstraction.

This paper has the purpose of determining the most probable reaction paths and the product distribution for the photo-oxidative degradation of toluene in aqueous media, to elucidate the effect of the water solvent on the reaction rate and on the subsequent formation of the primary intermediates. To this purpose, a combination of experimental and quantum mechanical methods were used. In the experimental part of the study, the formation yields of hydroxylated intermediates and of benzaldehyde were measured, in the presence of nitrate under UVB irradiation as the $\bullet\text{OH}$ source. Modeling of the reaction paths was performed using density functional theory (DFT) calculations to investigate the most plausible mechanism for the initial $\bullet\text{OH}$ attack and to determine the identities of the primary intermediates. Rate coefficients for all the reaction paths were computed by the Transition State Theory (TST) to obtain the product distribution. The effect of solvent water was investigated by using COSMO as the solvation model. Finally, the significance for surface waters of the reaction between toluene and $\bullet\text{OH}$ was studied by use of a recently developed photochemical model that foresees the lifetime of a compound upon reaction with $\bullet\text{OH}$, as a function of the reaction rate constant, the chemical composition and absorption spectrum of the surface water layer, and the water column depth (Vione et al., 2009 and 2010).

2. EXPERIMENTAL DETAILS

2.1 Reagents and materials

Toluene (for residue analysis) was purchased from Fluka, benzaldehyde (>99.5%) and H_3PO_4 (85%) from Aldrich, *o*-cresol (99%), *p*-cresol (99%) and benzoic acid (98%) from Carlo Erba, *m*-cresol (98%) and NaNO_3 (99%) from Merck, acetonitrile (Supergradient grade) from Scharlau. All reagents were used as received, without further purification. Water used was of Milli-Q quality (>18 $\text{M}\Omega\text{ cm}^{-1}$, TOC \approx 2 ppb).

2.2 Irradiation experiments

Solutions to be irradiated (5 mL total volume), containing 1 mM toluene and 0.1 M NaNO₃ (pH ≈ 6.5, measured with a Metrohm 713 pH meter equipped with a combined glass electrode), were placed into cylindrical Pyrex glass cells (4.0 cm diameter, 2.3 cm height). The solutions were magnetically stirred during irradiation, which was carried out under a 100 W Philips TL 01 lamp with emission maximum at 313 nm. The lamp had an irradiance of 5.0±0.2 W m⁻², measured with a CO.FO.ME.GRA. (Milan, Italy) power meter and corresponding to a photon flux of (3.3±0.1)×10⁻⁶ einstein L⁻¹ s⁻¹ in the solutions, actinometrically determined with the ferrioxalate method (Kuhn et al., 2004). Figure 1(a) reports the lamp emission spectrum, taken with an Ocean Optics SD 2000 CCD spectrophotometer and normalized to the actinometry data, also taking the transmittance of the Pyrex glass into account. The figure also reports the absorption spectrum of nitrate, measured with a Varian Cary 100 Scan UV-Vis spectrophotometer. Nitrate under UVB irradiation was used as the •OH source to induce the transformation of toluene (Mack and Bolton, 1999). Note that toluene does not absorb radiation in the wavelength interval of the lamp, and that no toluene transformation was detected in the dark in the presence of nitrate.

2.3 Analytical determinations

After irradiation, the solutions were analyzed with a Merck-Hitachi High Pressure Liquid Chromatograph equipped with AS2000A autosampler, L-6200 and L-6000 pumps for high-pressure gradients, L-4200 UV-Vis detector, and a RP-C18 LichroCART column (Merck, length 125 mm, diameter 4 mm) packed with LiChrospher 100 RP-18 (5 μm diameter). Elution was carried out with a 45:55 mixture of acetonitrile: aqueous H₃PO₄ (pH 3), at a flow rate of 1.0 mL min⁻¹. Injection volume was set at 100 μL, detection wavelength at 210 nm. Under these conditions the retention times were (min): benzoic acid (2.60), *m*- and *p*-cresol (3.65), *o*-cresol (4.00), benzaldehyde (4.15), toluene (14.40). The column dead time was 0.90 min. The perfect co-elution of *m*- and *p*-cresol caused some problems, but they showed similar slopes in the calibration curve. For this reason, the sum of the concentrations of *m*- and *p*-cresol is reported in the parts that follow.

2.4 Kinetic data treatment

The concentration vs. time data of toluene and its transformation intermediates are the average results of a run carried out in triplicate. The time evolution data of toluene were fitted with equation (1):

$$C_t = C_o \exp(-k_{tol}^d t) \quad (1)$$

where C_t is the concentration of toluene at the time t, C_o its initial concentration, and k_{tol}^d the pseudo-first order degradation rate constant. The initial transformation rate of toluene is

$R_{tol} = k_{tol}^d C_o$. The time evolution of each transformation intermediate was fitted with equation (2):

$$C_{int,t} = \frac{k_{int}^f C_o [\exp(-k_{tol}^d t) - \exp(-k_{int}^d t)]}{k_{int}^d - k_{tol}^d} \quad (2)$$

where C_o , k_{tol}^d and t are as above, $C_{int,t}$ is the concentration of the transformation intermediate at the time t , and k_{int}^f , k_{int}^d are the pseudo-first order formation and transformation rate constants of the intermediate, respectively. The initial formation rate of each intermediate is $R_{int} = k_{int}^f C_o$. The errors associated to the rates ($\mu \pm \sigma$) represent the scatter of the experimental data around the fitting curve. The yields of the different intermediates were derived from the ratio of their initial rates to that of toluene, as $\eta_{int} = R_{int} R_{tol}^{-1}$.

3. COMPUTATIONAL SET-UP AND METHODOLOGY

3.1 Computational Models

The molecular models were created by using the mean bond distances, the geometric parameters of the benzene ring, tetrahedral angles for sp^3 -hybridized carbon and oxygen atoms, and 120° for sp^2 -hybridized carbon atoms. In the calculation of the hydroxylated radicals, the aromatic ring was left planar except for the position of attack, and the attacking $\bullet OH$ radical was assumed to form a tetrahedral angle with the C-H bond.

3.2 Methodology

The reaction system under consideration consists of $\bullet OH$ radicals, in other words open-shell species. It is well-known that open-shell molecules pose severe problems in quantum mechanical calculations. Hartree-Fock (HF) methods suffer from spin contamination, because they are wave-function based. Therefore, they do not give accurate results. In contrast to the HF methods, DFT methods use the exact electron density instead of the wave function to calculate molecular properties and energies. Electron correlation, whose absence is the main drawback to HF methods, is accounted for in DFT methods. They do not suffer from spin contamination, and this feature makes them suitable for calculations involving open-shell systems. Therefore, geometry optimizations of the reactants, the product radicals, pre-reactive and the transition state complexes were performed with the DFT method within the GAUSSIAN 03 package (Frisch et al. 2003). The DFT calculations were carried out by the hybrid B3LYP functional, which combines HF and Becke exchange terms with the Lee-Yang-Parr correlation functional.

Choice of the basis set is very important in such calculations. In previous studies, radical addition reactions have been studied to determine the level of theory necessary for

predicting energy barriers, and B3LYP/6-311+G(d,p)//B3LYP/6-31G(d) has been found to be the most suitable (Wong and Radom, 1998; Ozen et al. 2003). Based on these results, optimizations in the present study were performed at the B3LYP/6-31G(d) level followed by single point energy calculations at the B3LYP/6-311+G(d,p) level. The forming C-O bonds in the addition paths and the H-O bond in the abstraction path were chosen as the reaction coordinates in the determination of the transition states. Ground-state and transition-state structures were confirmed by frequency analyses at the same level. Transition structures were characterized by having one imaginary frequency that belonged to the reaction coordinate, corresponding to a first-order saddle point. Zero-point vibrational energies (ZPEs) were calculated at the B3LYP/6-31G(d) level. The same ZPEs were used for the B3LYP/6-311+G(d,p)//B3LYP/6-31G(d) calculations. IRC calculations were performed for all of the transition geometries, and the corresponding maxima were confirmed.

3.3 Solvent Effect Model

In aqueous media, water molecules affect the energetics of the degradation reactions of all organic compounds. Moreover, water molecules induce geometry relaxation on the solute molecules. This effect on the geometry relaxation becomes more important when hydrogen-bonded complexes are present. However, the results obtained in earlier studies indicate that geometry changes have a negligible effect on the energy of the solute in water for both open and closed shell structures (Andzelm et.al. 1995, Barone and Cossi, 1998). Therefore, in this study, in order to take into account the effect of solvent H₂O on the energetics and the kinetics of the toluene + •OH reactions, DFT/B3LYP/6-311+G(d,p) calculations were carried out for the optimized structures of the reactants, the pre-reactive and the transition state complexes and the product radicals, by using COSMO (conductor-like screening solvation model) (Barone and Cossi, 1998) as the solvation model, implemented in the GAUSSIAN 03 package. The solvent was water at 25° C, with dielectric constant $\epsilon = 78.39$.

COSMO is one of the polarizable continuum methods (PCMs). In PCMs, the solute molecule is placed in a cavity surrounded by a polarizable continuum, whose reaction field modifies the energy and the properties of the solute (Hush et.al. 2005). The geometry of the cavity is determined by the shape of the solute. The reaction field is described in terms of apparent polarization charges or reaction field factors included in the solute Hamiltonian, so that it is possible to perform iterative procedures leading to the self – consistence between the solute wave-function and the solvent polarization. The COSMO method describes the solvent reaction field by means of apparent polarization charges distributed on the cavity surface, which are determined by imposing that the total

electrostatic potential cancels out on the surface. This condition can describe the solvation in polar liquids. Hence, it is the method of choice in this study.

4. RESULTS AND DISCUSSION

4.1 Photooxidation upon Nitrate Irradiation

Figure 1(b) reports the time evolution of 1.4 mM toluene and of its identified transformation intermediates (*o*- and *m*- + *p*- cresol, benzaldehyde), upon UVB irradiation of 0.10 M NaNO₃. Interestingly, no formation of benzoic acid took place in the studied system at the adopted irradiation time scale (up to 4 hours). The relevant values of R_{tol} , R_{int} and η_{int} are presented in Table 1.

Note that all the detected intermediates are compatible with a reaction between toluene and $\bullet\text{OH}$. The radical would mainly attack the aromatic ring of toluene to produce the cresols (hydroxymethylbenzenes) with a total yield of (78±16)%, while benzaldehyde would derive from the attack of $\bullet\text{OH}$ on the methyl group, with a yield of about 17±3%. Evidence that $\bullet\text{OH}$ is involved in the formation of benzaldehyde from toluene has been obtained both in the gas phase (Atkinson, 1994, and references therein) and in aqueous solution (Wang et al., 2009).

To make a comparison, in the gas phase the benzaldehyde yield from toluene + $\bullet\text{OH}$ is reported to be 5-10%, while the cresols are formed in 20-30% yield (with *o*-cresol strongly prevailing over the *m*- and the *p*- isomers). Other intermediates detected in the gas phase include benzyl nitrate and *m*-nitrotoluene, but their formation would mainly be a consequence of the atmospherically relevant conditions chosen in the experiments (e.g. presence of $\bullet\text{NO}$ and significant gas-phase nitration with $\bullet\text{OH} + \bullet\text{NO}_2$) (Atkinson, 1994, and references therein). If only the common intermediates of the reactions in the gas phase and in water are considered, it can be seen that in both cases the $\bullet\text{OH}$ attack on the ring prevails over that on the methyl group.

4.2 Computational Modeling

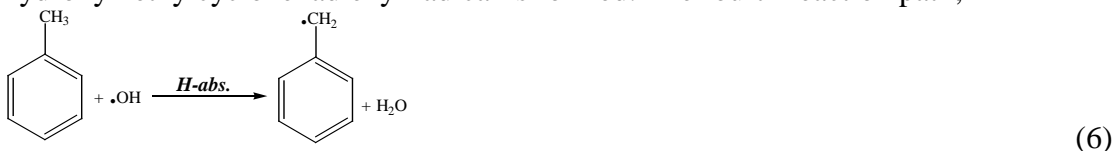
4.2.1 Reaction Paths

The hydroxyl radical is a very active species and has a strong electrophilic character (Brezová et.al. 1991). Once formed, it can readily attack the toluene molecule and produce the reaction intermediates. $\bullet\text{OH}$ radical reactions with aromatic compounds proceed mainly by two reaction pathways: H-atom abstraction from C-H bonds and addition to aromatic rings (Kilic et al. 2007). Based on the previous results (Uc et al. 2000, Suh et al. 2002, Seta et al. 2006,), four different reaction paths for the reaction of toluene with the $\bullet\text{OH}$ radical

were determined by nature of the carbon atoms of the ring and the methyl group. The first three reaction paths, *ortho*-addition (*o*-add), *meta*-addition (*m*-add) and *para*-addition (*p*-add) are shown below:



The $\cdot\text{OH}$ radical attacks a ring carbon with its unpaired electron and upon contact forms a C-O bond, while a π -bond of the aromatic system is broken and a hydroxymethylcyclohexadienyl radical is formed. The fourth reaction path;



consists in H-abstraction (H-abs) from the methyl group to produce a benzyl radical and a water molecule. The process of H-abstraction by the $\cdot\text{OH}$ radical is a simple atom-transfer reaction in which the bond to the carbon atom in the $-\text{CH}_3$ group is broken and a new bond to the oxygen atom of the $\cdot\text{OH}$ radical is formed.

4.2.2 Reactants and Product Radicals

Four different radicals were determined as the products of the reaction between toluene and the $\cdot\text{OH}$ radical. The electronic and thermodynamic properties for the most stable conformers were also calculated. Figure 2 represents the potential energy profile of the DFT-modeled mechanism for the initial attack of the $\cdot\text{OH}$ radical to toluene.

The total energies for each of the reactants and the product radicals obtained for both gas and aqueous media (Figure 2) indicate that the radicals, *o*-R, *m*-R and *p*-R produced in the addition paths are more stable than the H-R produced in the abstraction path. The reason may be attributed to the fact that all the radicals produced in the addition paths have hydrogen-bond-like stabilizations. The interaction distance between the original hydrogen atom at the addition center and the oxygen atom of the added $\cdot\text{OH}$ was calculated to be 1.997 Å for *m*-R and *p*-R, while it is 1.999 Å for *o*-R. For the gas phase, among the three radicals produced in the addition paths, *o*-R radical having the lowest energy is the most stable one. The *p*-R is around 0.3 and *m*-R is around 1.8 kcal.mol⁻¹ less stable than

the *o*-R. The energy of H-R is too high to be compared with the energies of the addition radicals. For the aqueous phase, the sequence remains the same. The most and the least stable radicals are again the *o*-R and the H-R, respectively. However, all the product radicals are more stable in the aqueous phase, due to the newly formed hydrogen bonds between the H atoms of the product radicals and the O atoms of the water molecules. The stabilities of the addition radicals increase by around 8.6 kcal.mol⁻¹. On the other hand, the difference in the gas and aqueous-phase energies for H-R was calculated to be 4.2 kcal mol⁻¹, much less than the former ones. This is consistent with the fact that H-R has less hydrogens, which causes weaker hydrogen bonding compared to the hydroxylated adducts.

By using the localization approach of the Wheland's approximation (Eberhard and Yoshida, 1973), it may be predicted that [•]OH addition is the most probable reaction path and that the positions of attack of the [•]OH radical are the *ortho* and *para* ones for both gas and aqueous phases. As seen in Figure 2, the products of the three addition paths lie ca. 15 kcal.mol⁻¹ below the reactants. Hence, it may be concluded that the reactions will proceed to the corresponding products, once the reactants are sufficiently close to each other. The thermodynamically most favored product is 1-hydroxy-2-methylcyclohexadienyl radical, followed by 1-hydroxy-4-methylcyclohexadienyl radical for both gas and aqueous phases.

4.2.3 Pre-reactive complexes

Our calculations indicated the formation of weakly-bound complexes between the [•]OH radical and toluene as the precursors of the reactions. Due to the existence of these pre-reactive van der Waals complexes, the reaction paths under investigation proceed over barriers that are lower in energy than the reactants. The pre-reactive complexes exert strong influence over the kinetics of the reactions by altering barrier heights and affecting the energy partitioning of the reaction products. Furthermore, the presence of such complexes affects the reaction dynamics by spatially directing the site of the reaction, either by steric direction or by providing a low potential well that favors a reaction site.

Depending on the direction of approach of the [•]OH radicals, four different chemically activated pre-reactive complexes, *o*-PC, *m*-PC, *p*-PC and H-PC with shallow wells, ca. 3 kcal.mol⁻¹ were determined for both gas and aqueous phases. The optimized structures of the pre-reactive complexes are shown in Figure 3. The [•]OH radical is seen to approach the aromatic ring from above, lying almost parallel to the ring plane with a deviation of about 5-10°. In the addition complexes, hydrogen atom was found to be facing towards the center of the ring, while the ring carbons at the addition centers were found to deviate from the ring plane by around 2°. The main difference in the optimized geometries occurs in the distance between the oxygen atom of [•]OH and the ring carbon. *m*-PC has much longer distance as compared with 1.9 Å in *o*-PC and 1.4 Å in *p*-PC. Energetically the *o*-PC and *p*-PC are the most stable complexes followed by H-PC, lying 3.27, 3.22 and 2.95

kcal.mol⁻¹ below the isolated reactants, respectively. The least stable pre-reactive complex is the *m*-PC, which is around 1.39 kcal.mol⁻¹ less stable than *o*-PC. It was observed that the stability of the pre-reactive complexes is higher in the aqueous than in the gas phase. The presence of water molecules, hydrogen-bonded to the hydrogen atoms of the complexes was found to lower the total energies. The reduction in energy was calculated to be ca. 6.65 kcal.mol⁻¹ for the three addition complexes and more ca. 8.24 kcal.mol⁻¹ for the H-PC. Although the energy gain of the reactants by complex formation is much less in water, the newly formed hydrogen bonds between the complex and the water molecules make the structures more stable.

4.2.4 Transition state complexes

Four transition state complexes *o*-TS, *m*-TS, *p*-TS and H-TS, one for each of the possible reaction paths were identified. The optimized structures of the TS are displayed in Figure 4. In all the complexes the [•]OH radical is oriented such that it is almost parallel to the ring plane, with slight deviations of ca. 0.5° in *p*-TS and H-TS, and 7° in *o*-TS and *m*-TS. The oxygen atom points to the carbon atom at the reaction center, while the hydrogen atom points to the center of the aromatic ring. The hydrogen atom at the addition center rotates out of the ring plane to the opposite side of the [•]OH, by 13.9°, 15.5° and 3.3° in *o*-TS, *m*-TS and *p*-TS respectively.

In the addition paths the major structural changes in the ring geometry relative to the parent toluene molecule are all localized around the carbon atom at the reaction center. The two C-C bonds connecting the addition center lengthen by 0.025-0.029 Å, whereas the change in the bond lengths of the subsequent bonds is lower, around 0.005 Å. This finding indicates that the two C-C bonds connecting the addition center have single rather than double bond character. The ones away from the addition center have a more pronounced double bond character. In the H-TS all the geometric changes are located around the methyl group and the carbon atom connecting it. Since a new bond is being formed between one of the hydrogen atoms of the methyl group and the oxygen atom of the [•]OH radical, H-C-H angles in the methyl group become narrower by 4°. There is also a slight elongation in the breaking bond, around 0.2 Å.

In the light of the potential energy profiles reported in Figure 2, it may be suggested that the forming bond length is a sensitive measure of the formation of the transition state complex along the reaction coordinate. As displayed in Figure 4, the addition complexes have much longer C-O bonds, 2.062 Å, 2.032 Å and 2.431 Å in *o*-TS, *m*-TS and *p*-TS, respectively, as compared to the C-O bonds in the corresponding radicals, 1.45 Å. This suggests that the addition complexes are early transition states, whereas the abstraction complex is formed late along the reaction coordinate. Among the three addition complexes the longest C-O bond belongs to the *p*-TS, while the *m*-TS and *o*-TS have much shorter C-

O bonds. This indicates that they are formed late as compared to *p*-TS and that, therefore, *p*-TS is the earliest transition state. Furthermore, the *p*-TS was found to have the lowest total energy among all the possible transition states (Figure 2), indicating that it is the most thermodynamically stable one. All the transition state structures, *p*-TS, *o*-TS, H-TS and *m*-TS lie 3.23, 2.89, 1.88 and 1.46 kcal.mol⁻¹, respectively, below the reactants. Thus, it may be concluded that in the photo-oxidative degradation of toluene, *p*-TS occurs early along the reaction coordinate, giving rise to a long C-O bond and a low total energy. As a consequence, it is the most probable transition state structure. It was observed that the stability order changes in the aqueous phase, where the H-TS has lower energy than *o*-TS. However, the stability of all the transition state structures increases due to weak interactions with the water molecules. Although the energies of all the transition state complexes decrease by around 7 kcal.mol⁻¹, the *p*-TS is the most thermodynamically stable TS for the aqueous phase as well.

4.2.5 Energetics of the reaction paths

The activation energies E_a for the four possible reaction paths were calculated and presented in Table 2 along with the reaction energies ΔE_r for both gas and aqueous phases. The values in Table 2 show that the activation energies for the three \bullet OH-addition paths are lower than for the H-abstraction path. The lowest activation energy belongs to the *para*-addition path. The energy barrier for the *ortho*-addition path is 0.37 kcal.mol⁻¹ higher than the energy barrier for the *para*-addition path. In the aqueous phase, the stability order of the transition state complexes changes in favor of *ortho*-addition. Although solvent water has a stabilizing effect in terms of total energies, the energy barriers in aqueous solution for *para*- and *meta*-addition paths are slightly higher than the barriers in gas phase. They increase by around 0.49 and 0.13 kcal.mol⁻¹ respectively, because of the prevention of the formation of the nice intramolecular hydrogen-bond network observed in the two transition state complexes. In contrast, the activation energy for the *ortho*-addition path decreases by around 0.12 kcal.mol⁻¹, causing the relevant reaction path to have the lowest activation energy among all the possible ones. In the aqueous phase, the barrier for H-abstraction also decreases by ca. 0.06 kcal.mol⁻¹. The reason may be attributed to the additional stabilizing effect of the newly formed hydrogen-bonds with the water molecules. Moreover, *para*- and *ortho*-addition paths were found to have the highest exothermicities in the gas phase, whereas the *ortho*-addition path has the highest exothermicity in the aqueous phase. The result is consistent with Hammond's postulate (Hehre et al. 1986), which states that early transition states have low energy barriers and high exothermicities. So, it may be concluded that *p*-TS and *o*-TS are the most probable transition states for gas and aqueous phases, respectively.

4.2.6 Reaction rates and product distribution

The rate constant k for each reaction path was calculated by using the Transition State Theory for 300 K. The classical rate constant k in the Transition State Theory is given by Eq. (7):

$$k = \frac{k_B T}{h} \frac{q_{TS}}{q_T \cdot q_{OH}} e^{-E_a / RT} \quad (7)$$

where k_B is Boltzmann's constant, T is temperature, h is Planck's constant, q 's are molecular partition functions for TS and the reactant species, toluene and $\bullet\text{OH}$, and E_a is the activation energy. Each of the molecular partition functions was assumed to be the product of translational, rotational, vibrational and electronic partition functions of the corresponding species.

The calculated rate constants in Table 2 show that in the gas phase the highest rate constant belongs to *para*-addition, followed by *ortho*- and *meta*-addition, whereas H-abstraction is the slowest reaction path, consistent with its high energy barrier. The branching ratio for each of the reaction paths was calculated by dividing the corresponding rate constant by the sum of the rate constants, taking the number of similar addition centers into account. By using the branching ratios, the relative concentrations of the primary intermediates were also calculated and are presented in Table 2. The results indicate that *ortho*-addition is the dominant reaction path for both gas and aqueous phases, followed by *para*-addition in gas phase, *meta*-addition in aqueous phase. Moreover, the calculated rate constants show that the *ortho*-addition and H-abstraction proceed faster in the aqueous phase compared to the gas phase. In contrast, the rates of the remaining paths decrease in aqueous solution, coherently with the increase in the energy barriers due to the weakening effect of water molecules on the original hydrogen bonds in the pre-reactive complexes.

The product distribution obtained indicates that the major primary intermediate formed in the photo-oxidative degradation of toluene is the *o*-R (1-hydroxy-2-methylcyclohexadienyl radical) which then forms *o*-cresol through abstraction of the redundant ring H by molecular oxygen. The reaction also yields *p*-R (1-hydroxy-4-methylcyclohexadienyl radical) and *m*-R (1-hydroxy-3-methylcyclohexadienyl radical). in lower amounts in water compared to the gas phase. The relative concentration of benzyl radical which is then converted to benzaldehyde through the reaction with O_2 is much less than all the other reaction products. The formation of benzaldehyde could be more favored in solution compared to the gas phase, but the solvent effect is relatively small and it is lower than the errors of the experimental data (Atkinson, 1994, and this work). The computational results indicate that the products of the photo-oxidative degradation of toluene are *o*-cresol (*o*-CR), *p*-cresol (*p*-CR), *m*-cresol (*m*-CR) and benzaldehyde (B), with

[*o*-CR] > [*p*-CR] > [*m*-CR] > [B] in the gas phase. The concentration order is [*o*-CR] > [*m*-CR] > [*p*-CR] > [B] in the aqueous phase, which is consistent with the experimental findings of this study.

4.3 Environmental Importance of Toluene Degradation

It is possible to foresee the half-life time of a water-dissolved compound CP because of reaction with $\bullet\text{OH}$ ($\tau_{\text{CP},\bullet\text{OH}}^{\text{SSD}}$), as a function of its second-order reaction rate constant with $\bullet\text{OH}$, $k_{\text{CP},\bullet\text{OH}}$, the chemical composition of the surface water layer (and in particular the concentration values of the main sources and sinks of $\bullet\text{OH}$), and the water column depth d . Note that d would be the average depth of thoroughly mixed water bodies or the mixing layer depth of large, stratified lakes. The half-life time units are summer sunny days (SSD), equivalent to a fair-weather 15 July at 45°N latitude. One gets $\tau_{\text{CP},\bullet\text{OH}}^{\text{SSD}}$ as follows (Vione et al., 2010):

$$\tau_{\text{CP},\bullet\text{OH}}^{\text{SSD}} = 1.9 \cdot 10^{-5} \cdot \frac{\sum_i k_{S_i} \cdot [S_i]}{R_{\bullet\text{OH}}^{\text{tot}} \cdot k_{\text{CP},\bullet\text{OH}}} \quad (8)$$

where $\sum_i k_{S_i} [S_i]$ is the rate constant of the natural $\bullet\text{OH}$ scavengers and $R_{\bullet\text{OH}}^{\text{tot}}$ is the formation rate of $\bullet\text{OH}$, which depends on the concentration of the main $\bullet\text{OH}$ sources (nitrate, nitrite and colored dissolved organic matter) and on the depth d of the water column. In the case of toluene it is $k_{\text{CP},\bullet\text{OH}} = 3.0 \times 10^9 \text{ M}^{-1} \text{ s}^{-1}$ (Buxton et al., 1988). A more complete description of the adopted photochemical model is reported as Supplementary Material (hereafter SM).

Figure 5(a) reports $\tau_{\text{CP},\bullet\text{OH}}^{\text{SSD}}$ for toluene in the presence of 2.1 mM bicarbonate and 26 μM carbonate, for $d = 1 \text{ m}$ and different concentration values of the dissolved organic matter (expressed as NPOC, Non-Purgeable Organic Carbon) and nitrate/nitrite. Nitrate was set to vary in the range of 1-30 μM , and it was hypothesized that $[\text{NO}_3^-]/[\text{NO}_2^-]=100$. Such a concentration ratio is reasonable in surface waters (Takeda et al., 2004; Minero et al., 2007). The half-life time for reaction with $\bullet\text{OH}$ is lower at higher nitrate and nitrite that are major $\bullet\text{OH}$ sources (nitrite is also a very minor $\bullet\text{OH}$ sink, but its role as scavenger is negligible compared to organic and inorganic carbon). Note the minimum of $\tau_{\text{CP},\bullet\text{OH}}^{\text{SSD}}$ for NPOC $\sim 1 \text{ mg C L}^{-1}$ in the presence of low nitrate and nitrite. The reason for the minimum is that, under such conditions, colored dissolved organic matter (CDOM) could prevail over nitrate/nitrite as $\bullet\text{OH}$ source and, at the same time, carbonate and bicarbonate would scavenge $\bullet\text{OH}$ to a comparable extent as organic matter itself. Therefore, for NPOC $< 1 \text{ mg C L}^{-1}$, the production of $\bullet\text{OH}$ by dissolved organic compounds would prevail over the scavenging. At elevated NPOC, the general increase of the half-life times is accounted for by the combination of $\bullet\text{OH}$ scavenging and radiation screening that are carried out by

dissolved organic matter. Figure 5(a) also reports the time interval that is hypothesized for the biological degradation of toluene in surface waters (1 to 6 months; Heald et al., 2005). It can be observed that the lifetime with $\bullet\text{OH}$ can be comparable to or even lower than that for the biological degradation, provided that nitrate and nitrite are present in sufficiently high concentration and that NPOC is not too high.

Figure 5(b) reports the expected time trends of 10 nM toluene ($\sim 1 \mu\text{g L}^{-1}$), cresols and benzaldehyde in the presence of 30 μM nitrate, 0.3 μM nitrite, 1 mg C L^{-1} NPOC, 2.1 mM bicarbonate and 26 μM carbonate, for $d = 1 \text{ m}$, under the hypothesis that all the compounds are formed and transformed upon reaction with $\bullet\text{OH}$ (the formation yields of the intermediates as reported in Table 1 were considered). The reaction rate constants with $\bullet\text{OH}$ of *o*-cresol, *p*-cresol and benzaldehyde are 1.1×10^{10} , 1.2×10^{10} and $4.4 \times 10^9 \text{ M}^{-1} \text{ s}^{-1}$, respectively (Buxton et al., 1988). The reaction rate constant of *m*-cresol is not reported but, given the similar values for the other two isomers, a reasonable approximation is to use the literature rate constant of *p*-cresol. Interestingly, all the transformation intermediates would be more reactive than toluene toward $\bullet\text{OH}$. By application of the model equation (8) and considering that $k_{CP}^d = 0.693 (\tau_{CP, \bullet\text{OH}})^{-1}$, under the hypothesized conditions it is $\tau_{\text{tol}, \bullet\text{OH}} = 47 \text{ SSD}$ ($k_{\text{tol}}^d = 1.5 \times 10^{-2} \text{ SSD}^{-1}$), $\tau_{\text{o-cr}, \bullet\text{OH}} = 13 \text{ SSD}$ ($k_{\text{o-cr}}^d = 5.4 \times 10^{-2} \text{ SSD}^{-1}$), $\tau_{\text{m-cr}, \bullet\text{OH}} = \tau_{\text{p-cr}, \bullet\text{OH}} = 12 \text{ SSD}$ ($k_{\text{m/p-cr}}^d = 5.9 \times 10^{-2} \text{ SSD}^{-1}$), and $\tau_{\text{benzald}, \bullet\text{OH}} = 32 \text{ SSD}$ ($k_{\text{benzald}}^d = 2.2 \times 10^{-2} \text{ SSD}^{-1}$). The time trend of toluene in Figure 5(b) was plotted with equation (1), that of the intermediates with equation (2). It can be seen that the concentrations of the intermediates would reach a maximum in approximately 50 SSD, and that the sum of their concentrations would never exceed 20% of the initial toluene. Note that benzaldehyde is the intermediate formed in lower yield but it is the most stable toward $\bullet\text{OH}$. The outcome is that benzaldehyde would be the most concentrated intermediate at long transformation times. Also note that the cresols could be transformed faster than foreseen by the adopted model, because they also undergo important reactions with the excited triplet states of CDOM (Canonica and Freiburghaus, 2001).

5. CONCLUSIONS

Photogenerated hydroxyl radicals by UVB irradiation of nitrate oxidize toluene by pseudo-first-order reaction rates. The experimental findings indicate that the radical $\bullet\text{OH}$ mainly attacks the aromatic ring of toluene to produce the cresols (hydroxymethylbenzenes) with a total yield of $(78 \pm 16)\%$, and benzaldehyde through the abstraction of a hydrogen atom from the methyl group, with a yield of about $17 \pm 3\%$. Based on the quantum mechanical calculations, four different reaction paths have been determined for the reaction of toluene with $\bullet\text{OH}$. DFT calculations indicate the formation of pre-reactive complexes between the

•OH radical and toluene as the precursors to the reaction. The addition complexes are early transition states, whereas the abstraction complex is formed late along the reaction coordinate. The activation energies for the addition paths are lower than the one for the abstraction path due to hydrogen-bonding. The presence of a dielectric continuum such as water increases the stabilities of all the species, but it also alters the energy barriers. In both gas and aqueous phases, the •OH attack on the ring prevails over that on the methyl group. Finally, •OH reaction could be a competitive sink for toluene in surface waters compared to microbial processes, in nitrate/nitrite-rich and DOM-poor water bodies.

Acknowledgements

The authors express their thanks to Yıldız Technical University Research Foundation (Project No : 24-01-02-15), PNRA-Progetto Antartide and MIUR-PRIN 2007 (2007L8Y4NB, Area 02, Project No: 36) for financial support.

REFERENCES

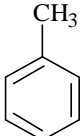
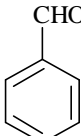
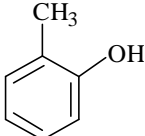
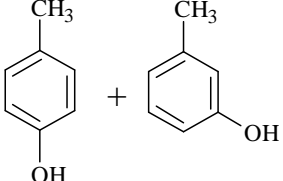
- Alvarez-Idaboy, J.R, Mora-Diez, N., Boyd, R.J., Vivier-Bunge, A., 2001. On the importance of prereactive complexes in molecule-radical reactions: hydrogen abstraction from aldehydes by OH. *J. Am. Chem. Soc.* 123 (9), 2018–2024.
- Andzelm, J., Kölmel., C., Klamt, A., 1995. Incorporation of solvent effects into density-functional calculations of molecular-energies and geometries. *J. Chem. Phys.* 103, 9312- 9320.
- Arambarri, I., Lasa, M., Garcia, R., Millan, E., 2004. Determination of fuel dialkyl ethers and BTEX in water using headspace solid-phase microextraction and gas chromatography-flame ionization detection. *J. Chromatogr. A* 1033, 193-203.
- Atkinson, R., 1994. Gas-phase tropospheric chemistry of organic compounds. *J. Phys. Chem. Ref. Data*, Gallagher, J. W. (ed.), Monograph n. 2.
- Barone, V., Cossi, M., 1998. Quantum calculation of molecular energies and energy gradients in solution by a conductor solvent model. *J. Phys. Chem. A* 102 (11), 1995–2001.
- Bekbolet, M., Çınar, Z., Kılıç, M., Uyguner, C.S., Minero, C., Pelizzetti, E., 2009. Photocatalytic oxidation of dinitronaphthalenes: Theory and experiment. *Chemosphere*, 75 (8), 1008- 1014.
- Bohn, B., 2001. Formation of peroxy radicals from OH-toluene adducts and O₂. *J. Phys. Chem.* 105, 6092-6101.

- Brezonik, P. L., Fulkerson-Brekken, J., 1998. Nitrate-induced photolysis in natural waters: Controls on concentrations of hydroxyl radical photo-intermediates by natural scavenging agents. *Environ. Sci. Technol.* 32, 3004-3010.
- Brezova', V., Ceppan, M., Brandsteterova, E., Breza, M., Lapcik, L., 1991. Photocatalytic hydroxylation of benzoic acid in aqueous titanium dioxide suspension. *J. Photochem. Photobiol. A: Chem.* 59 (3), 385-391.
- Bruno, P., Caselli, M., De Gennaro, G., Scolletta, L., Trizio, L., Tutino, M., 2008. Assessment of the impact produced by traffic source on VOC level in the urban area of Canosa di Puglia (Italy). *Water Air Soil Pollut.* 193, 37-50.
- Buxton, G.V., Greenstock, C.L., Helman, W.P., Ross, A.B., 1988. Critical Review of Rate Constants for Reactions of Hydrated Electrons, Hydrogen Atoms and Hydroxyl Radicals ($\bullet\text{OH}/\bullet\text{O}^-$) in Aqueous Solution. *J. Phys. Chem. Ref. Data* 17, 1027-1284.
- Canonica, S., Freiburghaus, M., 2001. Electron-rich phenols for probing the photochemical reactivity of freshwaters. *Environ. Sci. Technol.* 35, 690-695.
- Eberhardt, M.K., Yoshida, M., 1973. Radiation-induced homolytic aromatic substitution. I. Hydroxylation of nitrobenzene, chlorobenzene, and toluene. *J. Phys. Chem.* 77 (5), 589-597.
- Fatta, D., Michael, C., Canna-Michaehdou, S., Christoulidou, M., Kythreotou, N., Vasquez, M., 2007. Pesticides, volatile and semivolatile organic compounds in the inland surface waters of Cyprus. *Desalination* 215, 223-236.
- Frankcombe, T.J., Smith, S.C., 2007. OH-initiated oxidation of toluene. 1. quantum chemistry investigation of the reaction path. *J. Phys. Chem. A.* 111, 3686-3690.
- Frisch, M.J., Trucks, G.W., Schlegel, H.B., Scuseria, G.E., Robb, M.A., Cheeseman, J.R., Montgomery Jr., J.A., Vreven, T., Kudin, K.N., Burant, J.C., Millam, J.M., Iyengar, S.S., Tomasi, J., Barone, V., Mennucci, B., Cossi, M., Scalmani, G., Rega, N., Petersson, G.A., Nakatsuji, H., Hada, M., Ehara, M., Toyota, K., Fukuda, R., Hasegawa, J., Ishida, M., Nakajima, T., Honda, Y., Kitao, O., Nakai, H., Klene, M., Li, X., Knox, J.E., Hratchian, H.P., Cross, J.B., Adamo, C., Jaramillo, J., Gomperts, R., Stratmann, R.E., Yazyev, O., Austin, A.J., Cammi, R., Pomelli, C., Ochterski, J.W., Ayala, P.Y., Morokuma, K., Voth, G.A., Salvador, P., Dannenberg, J.J., Zakrzewski, V.G., Dapprich, S., Daniels, A.D., Strain, M.C., Farkas, O., Malick, D.K., Rabuck, A.D., Raghavachari, K., Foresman, J.B., Ortiz, J.V., Cui, Q., Baboul, A.G., Clifford, S., Cioslowski, J., Stefanov, B.B., Liu, G., Liashenko, A., Piskorz, P., Komaromi, I., Martin, R.L., Fox, D.J., Keith, T., Al-Laham, M.A., Peng, C.Y., Nanayakkara, A., Challacombe, M., Gill, P.M.W., Johnson, B., Chen, W., Wong, M.W., Gonzalez, C., Pople, J.A., 2003. *Gaussian 03*, B01. Gaussian Inc., Pittsburgh, PA.

- Heald, P.C., Schladow, S.G., Reuter, J.E., Allen, B.C., 2005. Modeling MTBE and BTEX in lakes and reservoirs used for recreational boating. *Environ. Sci. Technol.* 39, 1111-1118.
- Hehre, W.J., Radom, L., Schleyer, P.R., Pople, J.A., 1986. *Ab initio Molecular Orbital Theory*. Wiley, New York.
- Hoigné, J., 1990. Formulation and calibration of environmental reaction kinetics: Oxidations by aqueous photooxidants as an example. In: Stumm, W. (Ed.), *Aquatic Chemical Kinetics*. John Wiley and Sons, New York, Chp. 2, pp. 43-70.
- Holdway, D., Heggie, D. T., 2000. Direct hydrocarbon detection of produced formation water discharge on the Northwest Shelf, Australia. *Estuar. Coast Shelf Sci.* 50, 387-402.
- Hush, N.S., Schamberger, J., Bacskay, G.B., 2005. A quantum chemical computational study of the relative stabilities of cis- and transplatinum dichloride in aqueous solution. *Coord. Chem. Rev.* 249, 299–311.
- Karacanjic, B., Skender, L., Karacic, V., 2006. Benzene, toluene, ethylbenzene, and isomeric xylenes in various water samples in Canada. *Bull. Environ. Contam. Toxicol.* 76, 458-463.
- Katsumata, p. T., Kastenbergh, W. E., 1996. Fate and transport of methanol fuel from spills and leaks. *Hazard. Waste Hazard. Mater.* 13, 495-498.
- Kılıç, M., Koçturk, G., San, N., Çınar, Z., 2007. A model for product distributions for the reactions of phenol derivatives with hydroxyl radicals. *Chemosphere.* 69, 9, 1396-1408.
- Kuhn, H. J., Braslavsky, S. E., Schmidt, R., 2004. Chemical actinometry. *Pure Appl. Chem.* 76, 2105-2146.
- Mack, J., Bolton, J. R., 1999. Photochemistry of nitrite and nitrate in aqueous solution: A review. *J. Photochem. Photobiol. A: Chem.* 128, 1-13.
- Minero, C., Chiron, S., Falletti, G., Maurino, V., Pelizzetti, E., Ajassa, R., Carlotti, M.E., Vione, D., 2007. Photochemical processes involving nitrite in surface water samples. *Aquat. Sci.* 69, 71-85.
- Ozen, A. S.;Aviyente, V. Klein, R. A. 2003. Modeling the oxidative degradation of azo dyes: A density functional theory study. *J. Phys. Chem. A.* 107, 4898-4907.
- Robinson, C., Brovelli, A., Barry, D. A., Li, L., 2009. Tidal influence on BTEX biodegradation in sandy coastal aquifers. *Adv. Water Resour.* 32, 16-28.
- Seta, T., Nakajima, M., Miyoshi, A., 2006. High-temperature reactions of OH radicals with benzene and toluene. *J. Phys. Chem. A.* 110, 5081-5090.
- Soh, S. C., Abdullah, M. P., 2007. Determination of volatile organic compounds pollution sources in Malaysian drinking water using multivariate analysis. *Environ. Monit. Assess.* 124, 39-50.

- Suh, I., Zhang, D., Zhang, R., Molina, L.T., Molina, M.J., 2002. Theoretical study of OH addition reaction to toluene. *Chem. Phys. Lett.* 364, 454-462.
- Takeda, K., Takedoi, H., Yamaji, S., Ohta, K., Sakugawa, H., 2004. Determination of hydroxyl radical photoproduction rates in natural waters. *Anal. Sci.* 20, 153-158.
- Tully, F.P., Ravishankara, A.R., Thompson, R.L., Nicovich, J.M., Shah, R.C., Kreutter, N.M., Wine, P.H., 1981. Kinetics of the reactions of hydroxyl radical with benzene and toluene. *J. Phys. Chem.* 85, 2262-2269.
- Uc, V.H., Cruz, I.G., Laguna, A.H., Bunge, A.V., 2000. New channels in the reaction mechanism of the atmospheric oxidation of toluene. *J. Phys. Chem. A*, 104, 7847-7855.
- Uc, V.H., Alvarez-Idaboy, J.R., Galano, A., Cruz, I.G., Bunge, A.V., 2006. Theoretical determination of the rate constant for OH hydrogen abstraction from toluene. *J. Phys. Chem. A* 110, 10155-10162.
- Vione, D., Khanra, S., Cucu Man, S., Maddigapu, P. R., Das, R., Arsene, C., Olariu, R. I., Maurino, V., Minero, C., 2009. Inhibition vs. enhancement of the nitrate-induced phototransformation of organic substrates by the $\bullet\text{OH}$ scavengers bicarbonate and carbonate. *Wat. Res.* 43, 4718-4728.
- Vione, D., Das, R., Rubertelli, F., Maurino, V., Minero, C., Barbati, S., Chiron, S., 2010. Modelling the occurrence and reactivity of hydroxyl radicals in surface waters: Implications for the fate of selected pesticides. *Intern. J. Environ. Anal. Chem.* 90, 258-273.
- Wang, X. Q., Wu, J. P., Zhao, M. W., Lv, Y. F., Li, G. Y., Hu, C. W., 2009. Partial oxidation of toluene in CH_3COOH by H_2O_2 in the presence of $\text{VO}(\text{acac})_2$ catalyst. *J. Phys. Chem. C* 113, 14270-14278.
- Wixtrom, R. N., Brown, S. L., 1992. Individual and Population Exposures to Gasoline. *J. Exposure Anal. Environ. Epidemiol.* 2, 23-78.
- Wong, M.W., Radom, L., 1998. Radical additions to alkenes: Further assessment of theoretical procedures. *J. Phys. Chem. A* 102, 2237-2245.

Table 1. Initial degradation rate of 1.4 mM toluene and initial formation rates of the detected intermediates

	Initial Rate (M.s⁻¹)	Yields (%)
	$(9.85 \pm 0.79) \times 10^{-9}$	94.5 ± 19.4^a
	$(1.67 \pm 0.19) \times 10^{-9}$	17.0 ± 3.3
	$(3.00 \pm 0.35) \times 10^{-9}$	30.5 ± 6.0
	$(4.63 \pm 0.62) \times 10^{-9}$	47.0 ± 10.1

(a) The yield shown for toluene is the sum of the yields of the intermediates and of the associated errors.

Table 2. Activation energies E_a , reaction energies E_r , rate constants and product distributions for the possible reaction paths

	<i>o</i> -Addition	<i>m</i> - Addition	<i>p</i> - Addition	<i>H</i> - Abstraction
<i>Gas phase</i>				
E_a (kcal mol ⁻¹)	0.38	0.41	0.01	1.07
E_r (kcal mol ⁻¹)	-15.50	-13.73	-15.20	Endothermic
k (cm ³ molecule ⁻¹ s ⁻¹)	7.61×10^{-14}	3.43×10^{-14}	9.80×10^{-14}	3.11×10^{-14}
Branching Ratio(%)	43.5	19.6	28.0	8.9
<i>Aqueous phase</i>				
E_a (kcal mol ⁻¹)	0.26	0.54	0.50	1.01
E_r (kcal mol ⁻¹)	-16.16	-13.61	-13.65	Endothermic
k (cm ³ molecule ⁻¹ s ⁻¹)	9.34×10^{-14}	2.74×10^{-14}	4.31×10^{-14}	3.41×10^{-14}
Branching Ratio(%)	58.6	17.2	13.5	10.7

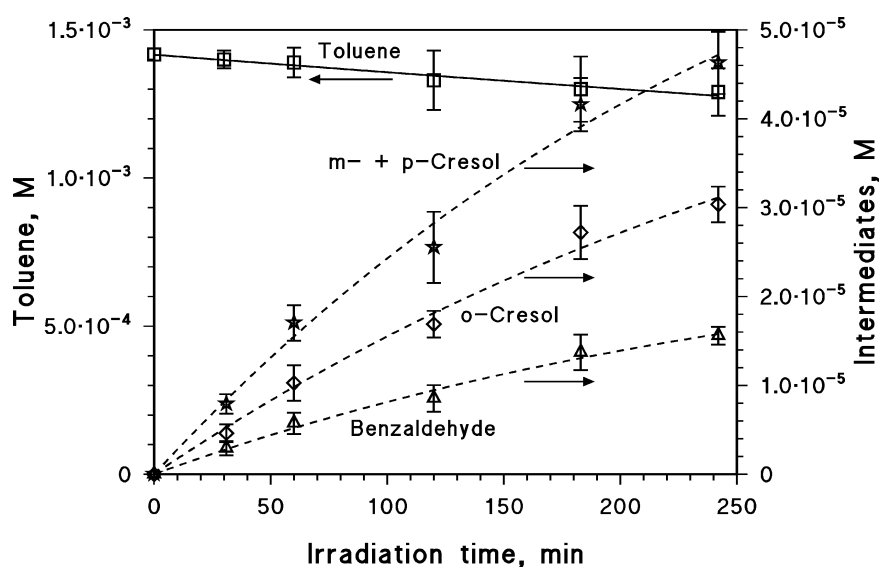
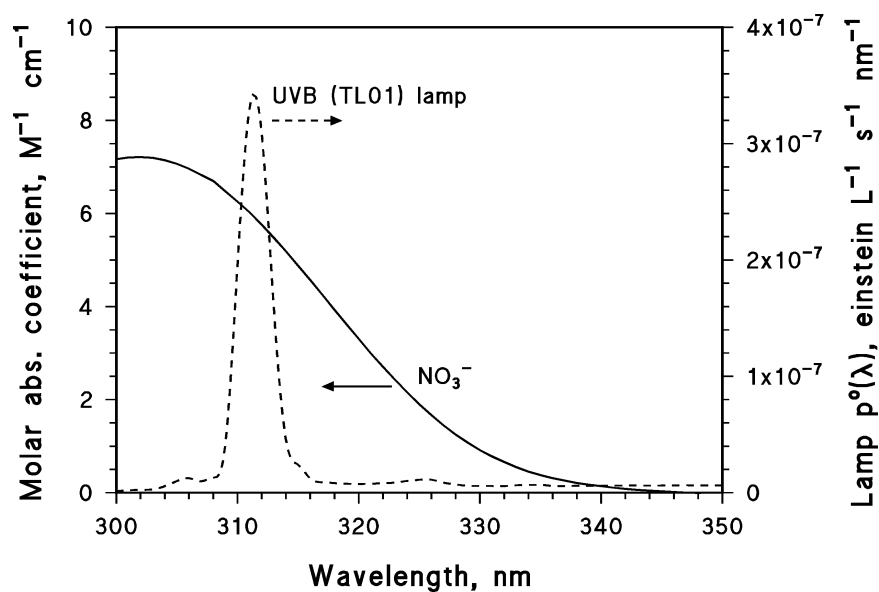


Figure 1. (a) Emission spectrum of the UVB lamp (Philips TL 01) adopted for the irradiation experiments. Molar absorption coefficient of nitrate.

Figure 1. (b) Time evolution of 1.4 mM toluene and of the detected transformation intermediates (cresols and benzaldehyde) upon UVB irradiation of 0.10 M NaNO_3 , pH ~ 6.

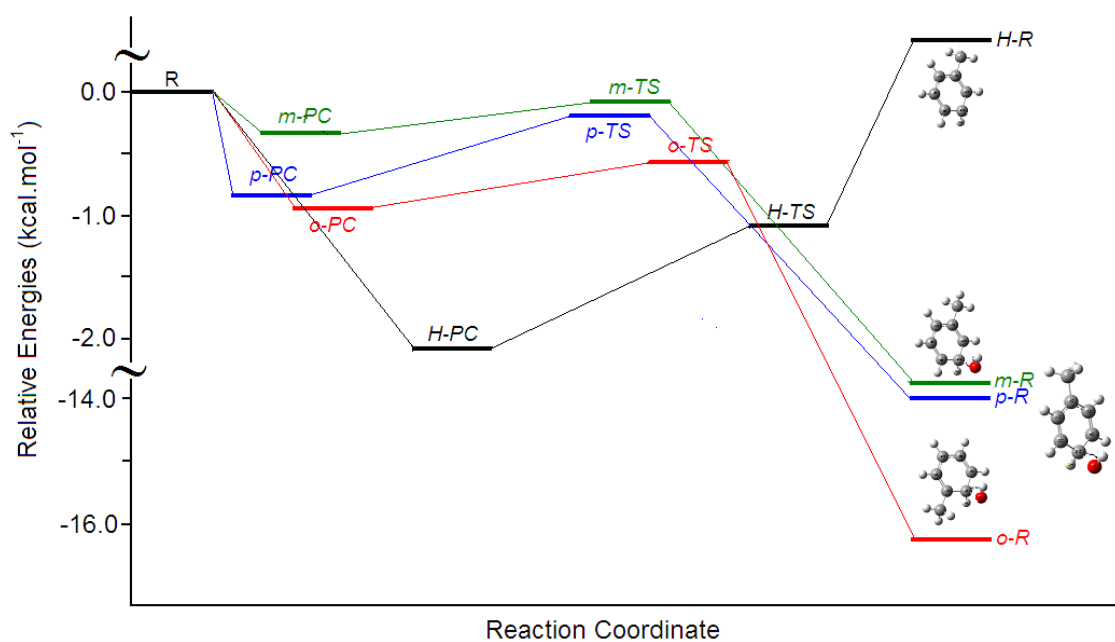
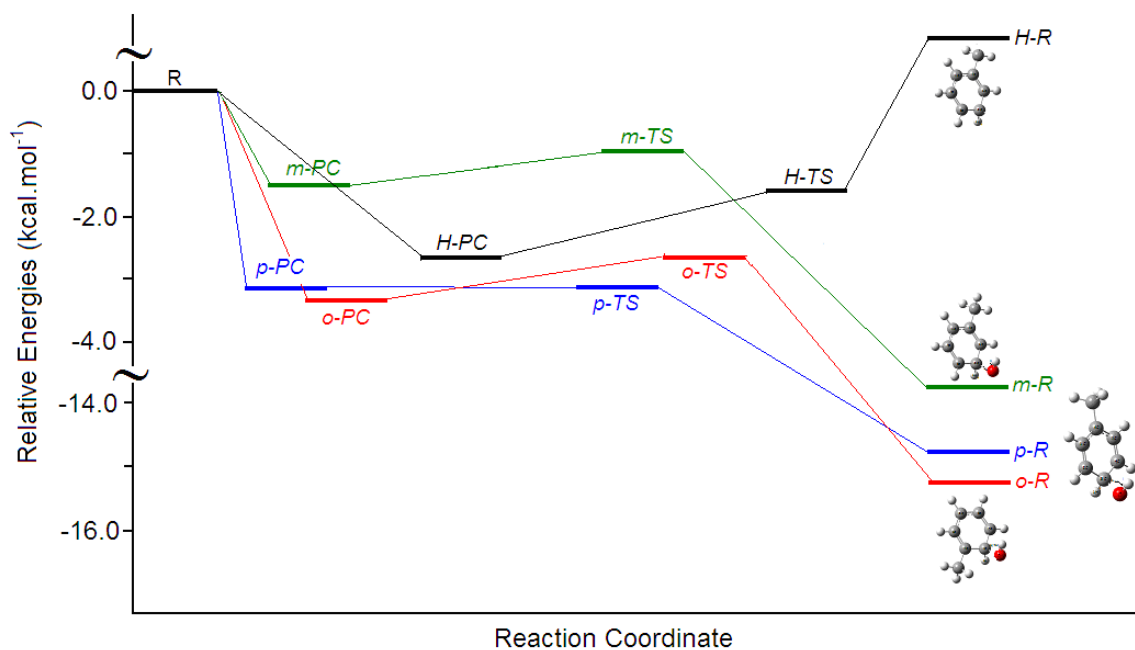
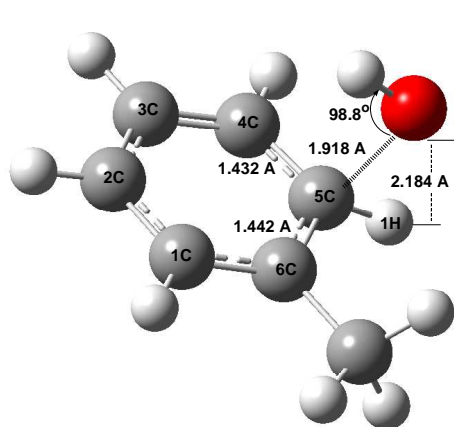
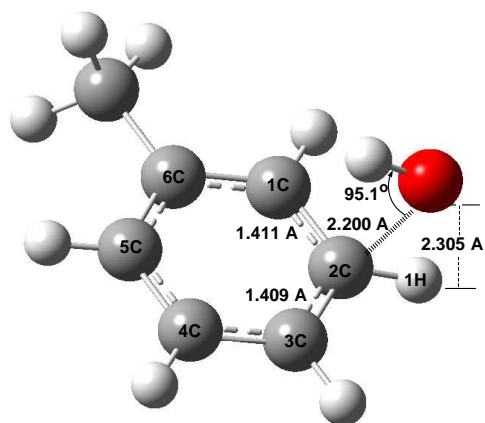


Figure 2. (a) The potential energy profile of the DFT-modeled mechanism for the Toluene+ OH reaction in gas phase.

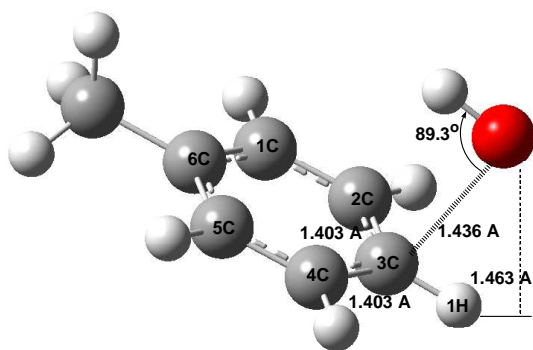
Figure 2. (b) The potential energy profile of the DFT-modeled mechanism for the Toluene+ OH reaction in aqueous phase.



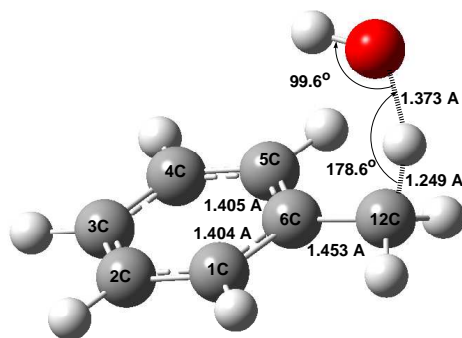
o-PC



m-PC



p-PC



H-PC

Figure 3

Figure 3. The optimized structures of the pre-reactive complexes.

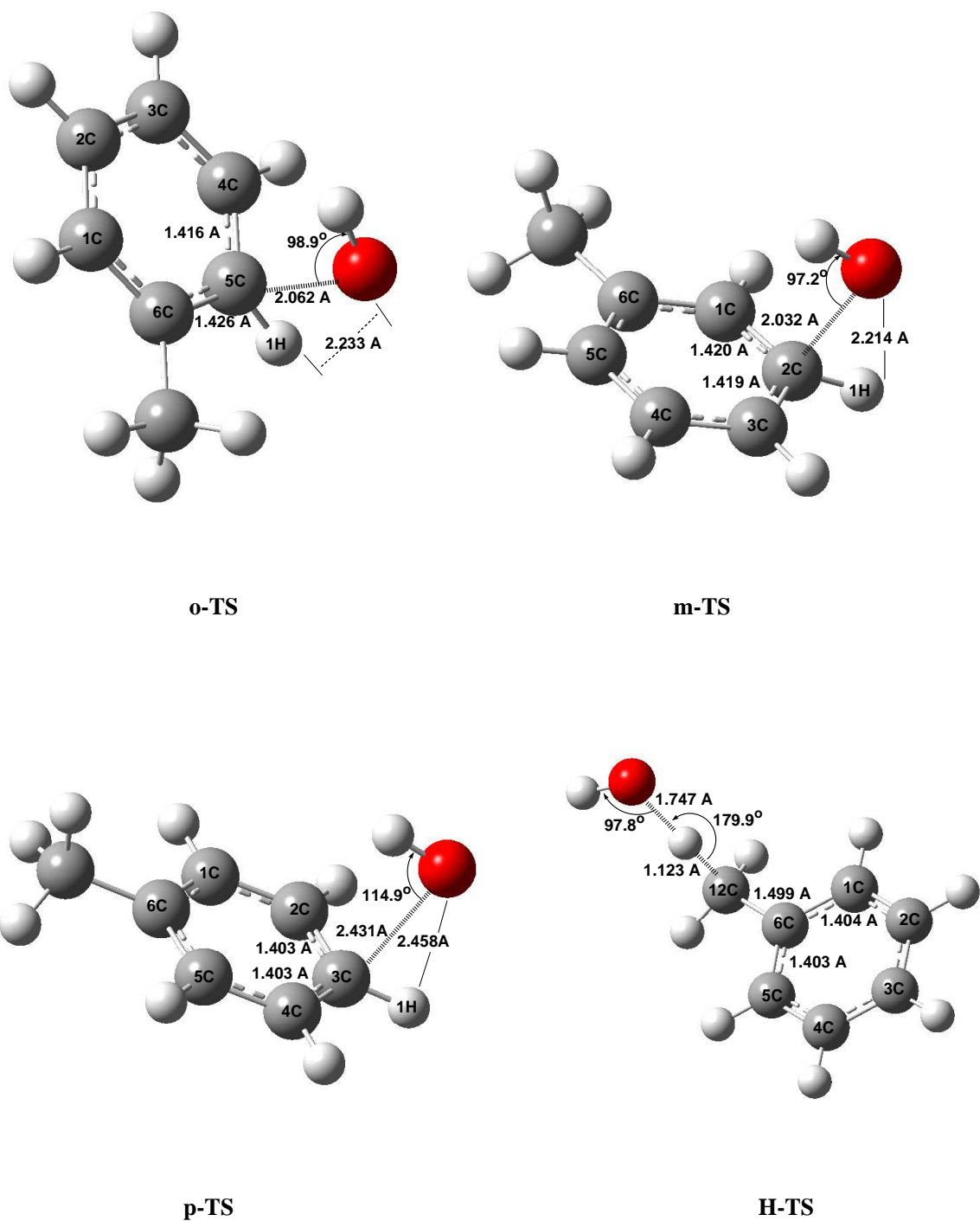


Figure 4

Figure 4. The optimized structures of the transition state complexes.

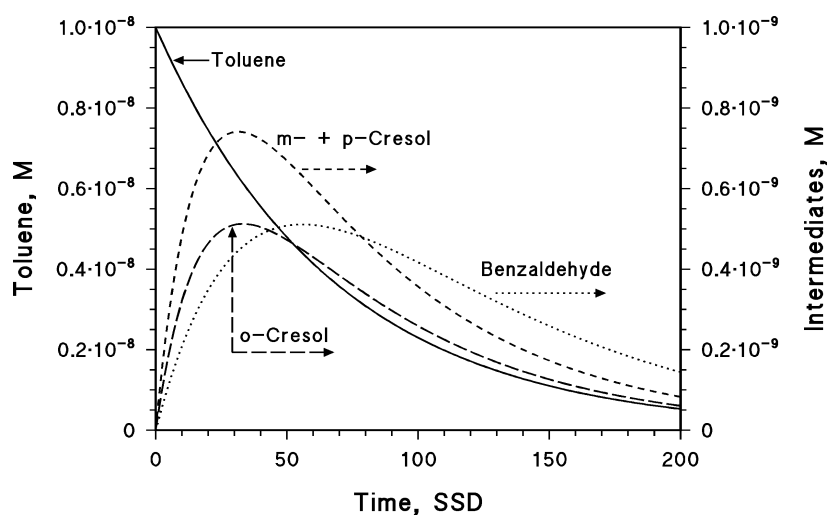
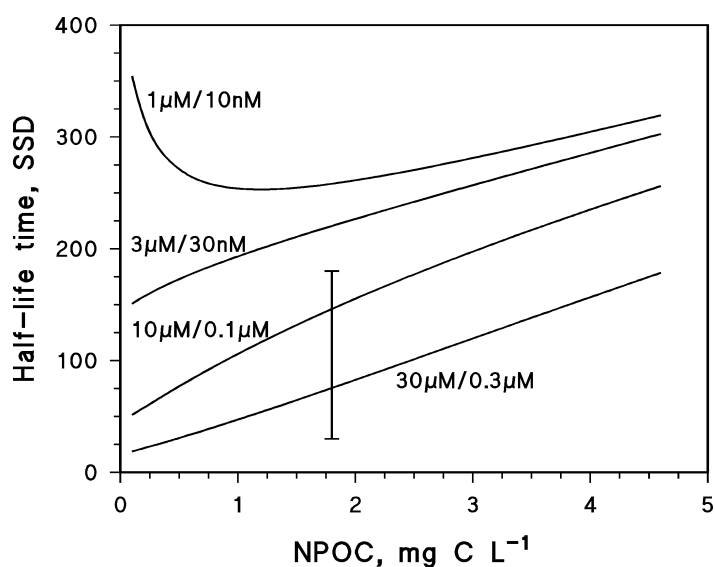


Figure 5. (a) Half-life time of toluene in the presence of 2.1 mM bicarbonate and 26 μM carbonate, for $d = 1$ m, as a function of $[\text{NO}_3^-]/[\text{NO}_2^-] = 100$ and of the NPOC. *the estimated lifetime for biological degradation is 1 to 6 months;* (Heald *et al.*, 2005).

Figure 5. (b) Time trend of toluene and of its main transformation intermediates upon reaction with $\bullet\text{OH}$, in the presence of 30 μM nitrate, 0.3 μM nitrite, 1 mg C L^{-1} NPOC, 2.1 mM bicarbonate and 26 μM carbonate, for $d = 1$ m, under the hypothesis that all the compounds undergo transformation with $\bullet\text{OH}$ alone.